ULTRASONIC IMAGING **32,** 190- 198 (2010)

Importance of Axial Compression Verification to Correct Interpretation of Axial-Shear Strain Elastograms in Breast Lesions

ARUN K. THITTAI, BELFOR GALAZ AND JONATHAN OPHIR

The University of Texas Medical School
Department of Diagnostic and Interventional Imaging
Ultrasonics Laboratory
Houston, TX
Jonathan.Ophir@uth.tmc.edu

We have recently shown that the appearance of Axial-Shear Strain Elastograms (ASSEs) for the case of loosely-bonded, elliptical inclusions (like fibroadenomas in the breast) is unique and therefore has the potential to distinguish benign fibroadenomas from malignant tumors in the breast. The ASSEs were obtained using quasi-static axial compressions, in a like manner as in normal axial-strain elastography. However, strict axial compression is achieved most often only by computer-controlled acquisitions and not by more practical freehand acquisitions. In a freehand acquisition, the frame sequence may contain several frames that do not experience strict axial compression but may also experience rotation or shear deformations. In this paper, we demonstrate the importance of accounting for the type of deformation applied to a target tissue for the correct interpretation of the resulting ASSEs. Using freehand acquired *in vivo* examples, we show that such a frame experiencing rotation or shear deformations results in ASSEs that may potentially be misinterpreted. This may be far more detrimental compared to the corresponding axial elastogram frames that may only suffer from inferior image quality in terms of contrast-to- noise ratio (CNR). Further, we show that we may be able to eliminate these frames from a sequence of freehand acquired *in vivo* breast lesion data by implementing a special filtering scheme, thus significantly improving the reliability of the remaining ASSE frames. This work further suggests that under freehand conditions, frames have to be checked for the presence of undesirable deformations.

KEY WORDS: Axial-shear strain; axial strain; benign breast disease; elastogram; elastography; fibroadenoma; frame filter; imaging; lesion; malignant; ultrasound.

INTRODUCTION

Ultrasound (US) elastography is now a well-established technique that utilizes frames obtained before and after a quasi-static compression to visualize the stiffness variations within inhomogeneous tissues.[1, 2] The image of the axial strain distribution due to quasi-static compression is commonly known as axial strain elastogram or axial elastogram.[1, 3, 4] We have shown that in addition to imaging the axial strain, one can image the axial-shear strain distribution at clinically-useful image levels.[5, 6] The image of the axial-shear strain due to quasi-static axial compression is referred to as an axial-shear strain elastogram (ASSE).[6, 7]

Using simulations, gelatin-phantom experiments and breast lesions *in vivo*, we have previously demonstrated that the axial-shear strain distribution patterns around an inclusion is directly influenced by tissue bonding at the inclusion-background boundary.[5, 6] In fact, results from the initial study to evaluate the potential of ASSEs to differentiate between fibroadenomas (thought to be loosely-bonded to surrounding host tissue)[8] and malignant tumors (thought to be firmly-bonded to the surrounding tissue)[8] in the breast have been very promising.[6] However, all prior work on ASSEs has assumed the inclusion shape to be circular.

We have recently demonstrated [9-11] in a series of finite-element simulations, experimentall validation in phantoms, as well as in initial examples from retrospective *in vivo* data that the axial-shear strain zones near firmly-bonded elliptical or elongated inclusions occur only out-

0161-7346/10 $18.00

side these inclusion. More importantly and clinically relevant, axial-shear strain zones occupy most of the interior portion of the inclusion exclusively in loosely-bonded elliptical inclusions that are inclined with respect to the compression axis, even at small not-normal orientations and that have even a slight eccentricity. The ASSEs obtained from the malignant and benign cases *in vivo* appeared to be in general agreement with our simulation and experimental results, suggesting that generating ASSEs of such lesions may have important implications. Specifically, axial-shear strain fill-in inside an inclusion may be a *unique signature* of loosely-bonded conditions at not-normal orientations of ellipsoidal or elongated inclusions. Thus, this fill-in may have potential as a marker of benignness of benign breast lesions (e.g., fibroadenomas) that are known to be stiff, elongated and loosely bonded to the host tissues. We postulate that the use of this specific signature may increase the negative predictive value (NPV) of standard practice ultrasound evaluations of benign breast lesions.

However, previous demonstrations of ASSE in tissue-mimicking phantom experiments and *in vivo* breast lesion examples utilized a computer-controlled digital motion controller (DMC) to apply precise axial compression.[5-7] In a practical clinical setting, one may desire a freehand acquisition instead. In such cases, there are several factors that influence the resulting elastographic quality (both axial and axial-shear strain). Over the last few years, several schemes have been proposed in the literature to improve the image quality of axial elastograms from sequence of freehand-acquired frames for real-time feedback[12-15] as well as near-real time offline processing.[16] More recently, Basarab et al[15] investigated the effect of the direction of axial compression on the axial elastogram frames that are acquired freehand from thyroid nodules. They showed that for frames in which the direction of axial compression was not nearly-axial, the resulting axial strain elastograms were of inferior CNR. They correctly argue that it is not uncommon to find several such frames in a sequence of freehand-acquired frames and therefore not eliminating these frames could degrade the whole scan sequence. We believe what was described as direction of axial compression therein could more broadly be described as type of deformation. Nevertheless, we hypothesize that such effect of the type of deformation on ASSE could have important consequences in the interpretation of axial-shear strain distributions. Therefore, it may become necessary to account for the type of deformation during postprocessing to reliably utilize ASSEs in a routine clinical setting.

In this paper, we will demonstrate the effect of the type of deformation on the resulting ASSE through examples from freehand-acquired *in vivo* breast lesion data. Thereafter, we describe a method to identify the type of deformation in an individual frame and a method for eliminating such frames from sequences of freehand-acquired frames.

MATERIALS AND METHODS

In vivo data acquisition and processing

The data used in this work were chosen from our existing rf database of *in vivo* breast fibroadenomas and cancers acquired freehand. In total, the database consisted of 33 cases but, at the time of this study, we had access to only about six cases at our location. The data were acquired at the University of Vermont by Brian Garra using a Sonix-500RP (Ultrasonix Medical Corporation, Richmond BC, Canada) scanner operating at 10 MHz. The number of cine-loop frames saved for each of the case differed but there were at least 200 frames in the cases used for this study. Further, some cases had more than one acquisition cine-loop saved and we randomly selected one such sequence. All the cases were histopathologically conirmed and patient identity removed. For the purposes of this pilot study, we identified example cases of a cancer and fibroadenoma that satisfied the following criteria: the sonographic

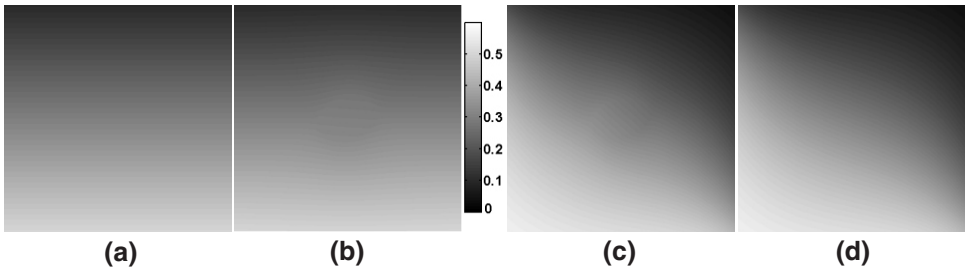

FIG. 1 Simulation showing example image of axial displacement that demonstrates the orientation of axial-displacement contour for (a, b) axial-compression and (c, d) axial-compression along with axial-shear deformation for (a, c) homogeneous and (b, d) inhomogeneous target.

lesion shape was approximately elliptical and the major axis of the lesion was not normally oriented with respect to the direction of compression. These criteria were chosen because of the potentially important and unique ASSEs for these cases, as demonstrated in our previous papers.[9-12]

Successive frames were treated as pre- and postcompression and the displacement map was computed using a proprietary multilevel coarse-to-fine 2D block matching algorithm implemented in Matlab®.[17, 9] The ASSEs were generated by extending the staggered-strain-estimation method as described in the referenced papers.[5, 18] A 5×5 median filtering scheme was applied to the displacement maps before estimating the ASSE.

Compression type identification

The axial displacement map obtained through finite-element modeling (FEM) for a homogeneous and inhomogeneous target when subjected to either axial compression deformation or axial-shear deformation is shown in figure 1 to demonstrate the difference in the orientation of the contour lines. Note that FEM was done using ANSYS® as detailed elsewhere.[5] Assuming that the US transducer (with/ without compressor plate) is used as a compression device in freehand acquisitions, a typical axial-displacement map within an elastically-homogeneous target subjected to axial compression will have displacement contour lines parallel to the surface (Fig. 1a). However, in the case of an inhomogeneous target, the parallels may be locally distorted around the inclusion (Fig. 1b). The displacement contour lines may not be parallel if the type of deformation experienced by the target differs from axial compression (Figs. 1c, d). Therefore, defining a metric for the deviation from parallelism of the displacement contour may provide a way to determine if the applied deformation constitutes the desired axial compression or an undesired deformation like shear or rotation. Note that the global shear or rotation due to improper external compression is undesirable, whereas the local shear or rotation due to the shape, orientation and boundary condition of the inclusion is the desired signature. Therefore, the metric that measures the deviation from parallelism of the displacement contour should be more sensitive globally than locally. The method we employed to estimate the average deviation from parallelism (ADP) is described below.

The displacement map at a fine-level from each frame is segmented into nine regions, as shown in figure 2 and subjected to the following computations:

$$\mathrm{Di} = \mathrm{mean}\left(\frac{|\, d_{i,1} - d_{i,2} \,|}{\max(|\, d_{i,1} \,|, |\, d_{i,2} \,|)}, \frac{|\, d_{i,2} - d_{i,3} \,|}{\max(|\, d_{i,2} \,|, |\, d_{i,3} \,|)}, \frac{|\, d_{i,3} - d_{i,1} \,|}{\max(|\, d_{i,3} \,|, |\, d_{i,1} \,|)} \right) \quad (1)$$

for $i = 1, 2, 3$.

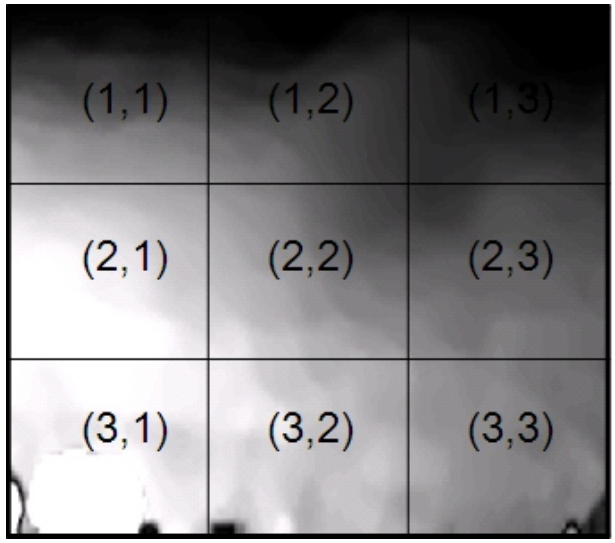

FIG. 2 Experimental example showing an image of axial displacement that demonstrates segmenting of the frame into 3×3 regions of benign breast fibroadenoma.

$$ADP = Max(D_i) \tag{2}$$

where $d_{i,j}$ is the average of all the axial displacement pixels in the region (i, j) that have corresponding correlation coefficient value >0.75. The threshold on the correlation coefficient was used to avoid low-quality displacement pixels from entering the computation. *D1*, *D2* and *D3* capture the difference between the average displacement values in regions located at different depths (Eq. (1)). The rationale behind the method is that the average displacement in each region at a particular depth will be similar for an axial compression and therefore will result in low values for *D1*, *D2* and *D3*. The maximum of these three values is used as a measure that indicates the amount of ADP (Eq. (2)). Note that ADP is normalized such that it ranges from 0 to 1. Clearly, values close to 0 indicate more parallel axial-displacement contour, as would be expected from an ideal axial compression, and are desirable.

Percentage fill-in of axial-shear strain inside lesion

Recall that as described in the reference 9, we would expect axial-shear strain fill-in only in loosely-bonded fibroadenomas that are elliptically-shaped, oriented lesions and are not in firmly-bonded malignant tumors when subjected to axial compression. Therefore, the presence or absence of axial-shear strain fill-in inside a lesion may be a unique signature of the type of lesion and its interpretation is critical. If there is fill-in of axial-shear strain that is not due to bonding conditions but rather to undesired tissue deformation, ASSEs may potentially be misinterpreted. Therefore, it becomes necessary to see the effect of deformation on the fill-in of axial-shear strains inside the lesion. In order to study this effect, we calculated the percentage area of the lesion that experienced axial-shear strain. This was calculated by using the formula

$$\%\,fill-in = \left(\frac{number\ of\ \ pixels\ greater\ than\ Axial\ shear\ strain\ threshold}{total\ number\ of\ \ pixels} \right) x100 \tag{3}$$

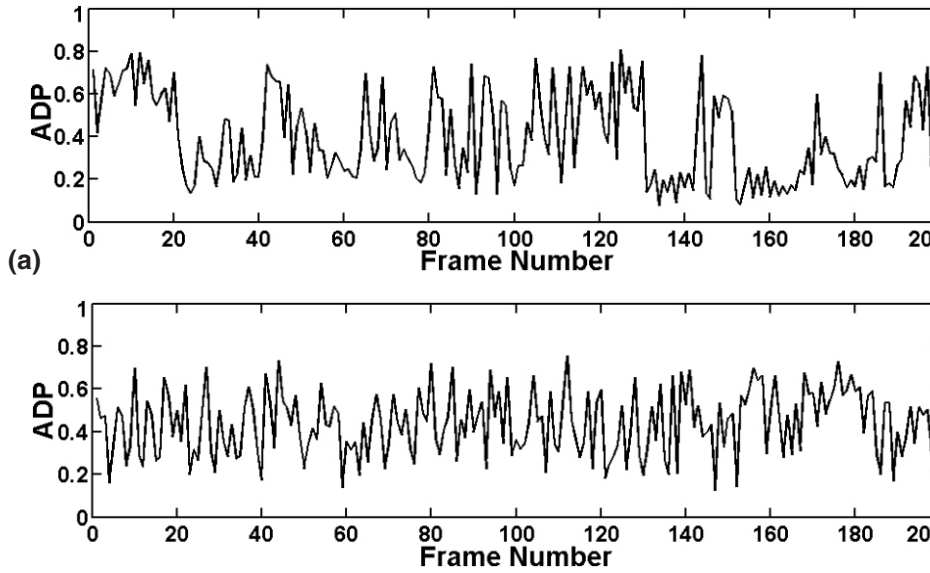

FIG. 3 Plot of the metric 'ADP' obtained for each frame of the freehand-aqcquired sequence from (a) fibroadenoma and (b) malignant tumor.

where the axial-shear strain threshold was arbitrarily chosen as 40% of the frame-average axial strain value. Here again, only pixels with corresponding correlation coefficient values greater or equal to 0.75 were included in the calculation.

The lesion area visible in the sonogram was outlined by one of the author (BG) and used in the computations. Note that the lesion outline can also be obtained from the corresponding axial elastogram if the sonographic lesion is not completely visible. However, in this paper, the cases chosen had an unambiguous sonographic lesion appearance.

Cine-loop postprocessing

The metric relating to the quality of the axial compression, ADP and percentage fill-in value were computed for each of the frames from the sequence of a freehand-acquired cine-loop. We implemented deformation filtering by imposing an arbitrary threshold on ADP. Apart from this filtering, one could implement various other postprocessing schemes to improve the elastographic (axial strain and axial-shear strain) image-quality of the cine loop.[15-17] However, the scope of the current work is limited to study the effect of the more fundamental deformation acquisition parameter on ASSEs. Therefore, we did not subject the frame sequence to any postprocessing beyond applying a persistence of six frames in order to smooth interframe jitter.

RESULTS AND DISCUSSION

Figure 3 shows a plot of the metric, ADP, for each of the 200 frames from an example case of a fibroadenoma and malignant tumor. This plot clearly demonstrates the existence of several frames that experienced rotation/shear deformation during supposedly freehand, purely-axial compression (indicated by the peaks).

Figure 4 shows the set of sonograms, axial-displacement map and ASSE from a representative frame at a low value of ADP (= 0.14 cancer; 0.18 fibroadenoma). Recall that a value of

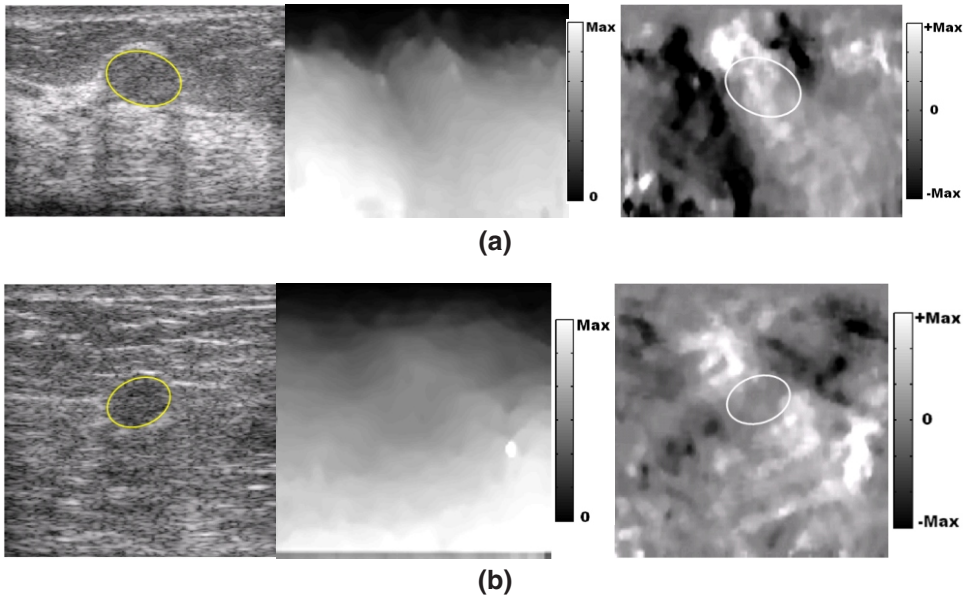

FIG. 4 (Left) sonograms, (center) axial displacement images and (right) ASSEs from a representative frame with low value for ADP from (a) fibroadenoma and (b) malignant tumor in the breast.

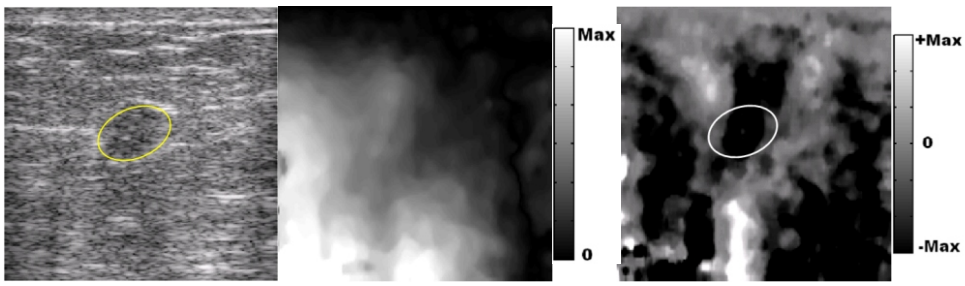

FIG. 5 (Left) sonogram, (center) axial displacement images and (right) ASSEs from a representative frame from malignant tumor case with high value for ADP. Observe a misleading fill-in of axial-shear strain inside the tumor due to the nature of the deformation.

ADP closer to 0 indicates a purer axial-compression. Observe that the displacement contour is parallel to the surface of compression, as is typical for axial-compression. Further, observe the presence of high-contrast margins of opposite polarity along with fill-in of axial-shear strain inside the lesion for the case of fibroadenoma. There is no such fill-in of axial-shear strain inside a malignant tumor (Fig. 4b). The ASSE shown here for a freehand-acquired frame is consistent with the ASSE reported earlier by Thittai et al[9] for the frames acquired through computer-controlled compression.

Figure 5 shows the set of sonograms, axial-displacement maps and ASSEs from a representative frame at a high value of *ADP* (= 0.65) for a malignant case. Observe that the displacement contour is not as parallel to the surface as the case shown in figure 4. It can be seen from the ASSEs that the fill-in of axial-shear strain occurs even in the case of malignant tumor. However, the axial-shear strain fill-in this case is most likely due to the axial-shear/rotation deformation applied (look at the axial displacement contours) and not due to lesion boundary bonding conditions. This image clearly demonstrates the need to consider the type of deformation to avoid misinterpretation of the ASSE.

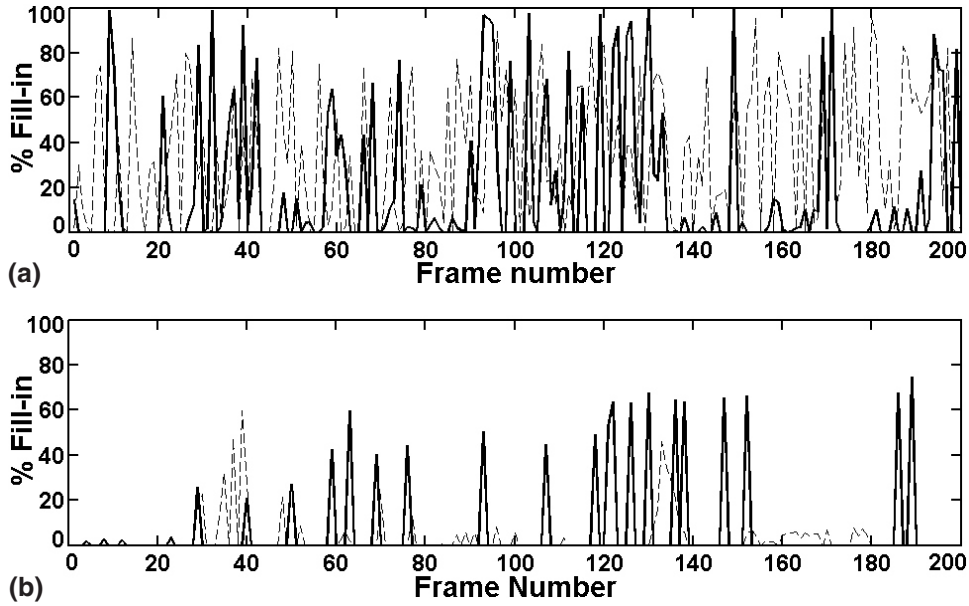

FIG. 6 Plot showing the percentage fill-in value for each of the frames (fibroadenoma (—) and malignant tumor (-)) (a) before and (b) after removing frames based on a threshold of 0.25 for 'ADP'.

Figure 6a shows a plot of the percentage fill-in value for each frame for the fibroadenoma and malignant tumor cases shown in figure 2. It can be seen that both the fibroadenoma and cancer have frames with high fill-in values but more such frames are found in the case of fribroadenoma. Figure 6b incorporates the effect of the type of deformation by eliminating frames that have ADP values greater than an arbitrary threshold of 0.25. Observe that most of the frames that had fill-in due to undesired deformation got removed in the case of malignant tumor. The cine-loop movie of these two cases is posted online: http://www.uth.tmc.edu/schools/med/rad/elasto/movies/index.htm.

Figure 7 summarizes the effect of ADP by showing the percentage of frames that have at least 50% fill-in at different thresholds for ADP. Note that for each value of *ADP* the number of frames that survive is different, i.e., smaller values imposes stricter criterion on the axial compression, resulting in fewer frames, while larger values are more lenient and allow capture of more frames. Obviously, the percentage of frames with fill-in will depend on operator training and experience as well as the fundamental model parameters of shape, orientation and lesion type. Nevertheless, it is clear that by appropriately accounting for the type of deformation by controlling the threshold of ADP, we could gain greater certainty for the interpretation of the ASSE.

CONCLUSIONS

We have demonstrated through example of freehand-acquired, breast-lesion data *in vivo* that the type of deformation plays an important role in the interpretation of the resulting ASSE. It is clear from the results that during freehand acquisition, there may be some frames that do not experience the ideally-intended quasi-static axial compression. We have shown that it is important to identify such frames (preferably in real-time) in order to improve the reliability of the cine loop and thus improve the diagnostic accuracy.

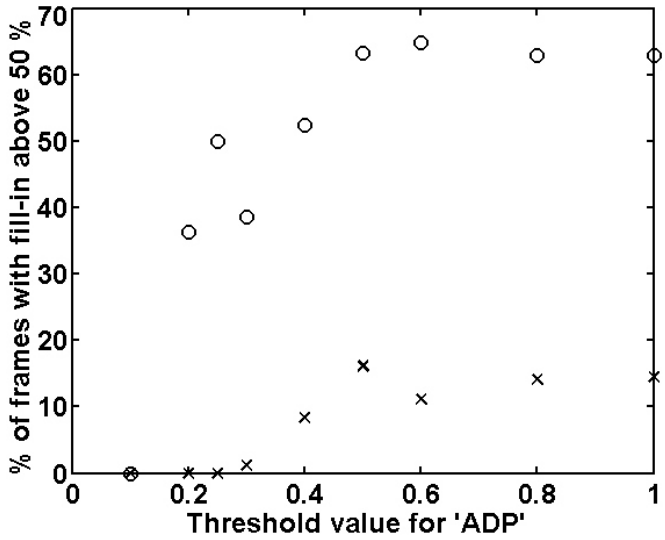

FIG. 7 Plot showing the percentage of frames that survive at a particular threshold of ADP and have at least 50% of lesion fill-in with axial-shear strain. Observe that for a threshold of 'ADP' around 0.2-0.3, the fill-in occurs only in fibroadenoma ('o') and not cancer ('x').

ACKNOWLEDGEMENT

This work was supported in part by NIH grants R21-CA135580-01 and 1R21CA12729101. The *in vivo* sonographic data were acquired and pathologically confirmed by Brian Garra, MD from the University of Vermont under a subcontract from the University of Texas with support from NIH Program Projects P01-CA64597 and P01 EB002105.

REFERENCES

1. Ophir J, Céspedes I, Ponnekanti H, et al. Elastography: a method for imaging the elasticity of biological tissues, *Ultrasonic Imaging 13,* 11-13 (1991).

2. O'Donnell M, Skovoroda AR, Shapo BM. Internal displacement and strain imaging using ultrasonic speckle tracking, *IEEE Trans Ultrasonics Ferroelec Freq Cont 41*, 314-325 (1994).

3. Ophir J, Alam SK, Garra BS, et al. Elastography: ultrasonic estimation and imaging of elastic properties of tissues, *Proc Instn Mech Engrs (UK) 213,* 203-233 (1999).

4. Céspedes I. Elastography: *Imaging of Biological Tissu*e Elasticity, *Ph.D. Dissertation*. (University of Houston, 1993).

5. ThitaiKumar A, Krouskop TA, Garra BS, Ophir J. Visualization of bonding at an inclusion boundary using axial-shear strain elastography: a feasibility study, *Phys Med Biol 52*, 2615-2633 (2007).

6. Thitaikumar A, Mobbs LM, Kraemer-Chant CM, Garra BS, Ophir j. breast tumor classification using axial shear strain elastography: a feasibility study, *Phys Med Biol 53*, 4809-4823 (2008).

7. ThitaiKumar A, Ophir J, Righetti R, Krouskop TA. Resolution of axial-shear strain elastography, *Phys Med Biol 51*, 5245-5257 (2006).

8. Fry KE. Benign Lesions of the breast, *CA Cancer J Clin 4*, 160-161 (1954).

9. Thittai AK, Galaz B, Ophir J. Axial-shear strain distributions in an elliptical inclusion model: experimental validation and *in vivo* examples with implications to breast tumor classification *Ultrasound Med Biol 36,* 814-820 (2010).

10. Galaz B, ThitaiKumar A, Ophir J. Axial-shear strain distribution in an elliptical inclusion model (Part I): a simulation study, in *Proc Eighth Internatl Conference Ultrason Measurement Imaging*, p. 99 (Vlissingen, Zeeland, Netherlands, 2009) (abstact only).

11. ThitaiKumar A, Galaz B, Ophir J. Axial-shear strain distribution in an elliptical model (Part II): Experimental validation and in vivo examples with implication to breast tumor classification, in *Proc Eighth Internatl Conference Ultrason Measurement Imaging*, p. 100 (Vlissingen, Zeeland, Netherlands, 2009)(abstact only).

12. Jiang J, T. Hall TJ, A. Sommer AM. A novel performance descriptor for ultrasonic strain imaging: a preliminary study, *IEEE Trans Ultrason Ferroelec Freq Contr 53*, 1088-1102 (2006).

13. Lindop JE, Treece GM, Gee AH, Prager RW. Frame filtering for improved freehand 3D US elastography, in *Proc Fourth Internatl Conference Ultrason Measurement Imaging*, p. 74 (Austin, TX, 2005).(abstact only)

14. Lindop JE, Treece GM, Gee AH, Prager RW. An Intelligent interface for freehand strain imaging. *Tech. Rept. CUED/F-INFENG/TR 578, (*Cambridge Univ. Dept. of Engineering, May, 2007).

15. Basarab A, Lyshchik A, Grava C, Buzuloiu V, Delachartre P. Ultrasound image sequence registration and its application to thyroid nodular disease. *J Sign Process Syst 55*, 127-137 (2009).

16. Jiang J, Hall TJ, Sommer AM. A novel image formation method for ultrasonic strain imaging. *Ultrasound Med Biol, 33*, 643-652 (2007).

17. Shi H, Varghese T. Two-dimensional multi-level strain estimation for discontinuous tissue. *Phys Med Biol 52*, 389-401 (2007).

18. Srinivasan S, Ophir J, Alam SK. Elastographic imaging using staggered strain estimates, *Ultrasonic Imaging 25*, 229-245 (2002).